J Low Temp Phys (2009) 154: 41–54
DOI 10.1007/s10909-008-9849-8

Experimental Observation of Fluxon Diffusion in Josephson Rings

K. Segall · A.P. Dioguardi · N. Fernandes · J.J. Mazo

Received: 16 July 2008 / Accepted: 16 October 2008 / Published online: 30 October 2008

Abstract We present switching current measurements in niobium-aluminum oxide-niobium underdamped Josephson rings. Underdamped Josephson rings display hysteretic current-voltage curves which can be characterized by their switching current, the value of applied current at which the junctions switch to the energy-gap voltage. The value of the switching current is strongly affected by temperature and by the presence of fluxons in the system. We observe a very small voltage (∼400 nV) across the ring prior to switching, indicating a low-velocity fluxon diffusion state before the jump to a full running state. In analogy with previous work on single junctions, we analyze the switching current data with the process of thermal activation over a dissipation barrier, where the system switches from a low velocity state to a high velocity state. We find that our data agrees qualitatively with this description, further supporting the observation of fluxon diffusion.

Keywords Josephson array · Fluxon · Josephson ring · Switching current · Thermal activation · Dissipation barrier · Phase diffusion

1 Introduction

Arrays of Josephson junctions have proven to be extremely interesting systems to study nonlinear and collective effects [1–3]. Previous work has focused mostly on

K. Segall (✉) · A.P. Dioguardi · N. Fernandes
Department of Physics and Astronomy, Colgate University, Hamilton, NY 13346, USA
e-mail: ksegall@mail.colgate.edu

J.J. Mazo
Dpto. de Física de la Materia Condensada, Universidad de Zaragoza and Instituto de Ciencia de Materiales de Aragón, C.S.I.C.-Universidad de Zaragoza, 50009 Zaragoza, Spain

three major geometries: the two-dimensional array [4], the Josephson ladder [5, 6], and the parallel array [7–9]. Of these the parallel array (or Josephson ring if it is closed in a circle), displays one-dimensional behavior and is an important component in RSFQ (Rapid-Single-Flux-Quantum) circuits. The main excitation in a Josephson ring is a fluxon, a discrete counterpart to the soliton. Fluxons in a Josephson ring obey the discrete Sine-Gordon equation and are analogous to kinks in the 1-D Frenkel-Kontorova model [10–13].

In overdamped Josephson rings, the current-voltage (I-V) curves are single valued. The dynamics of fluxons trapped in the ring are straightforward to infer in those cases because the voltage, which is directly proportional to the fluxon velocity, has a unique value at each current. Underdamped arrays display a richer variety of behavior but are more difficult to analyze, since the I-V curves are bistable. In many previous experiments on single junctions, *switching current* measurements have been utilized to study the dynamics of the Josephson phase when the I-V curves are bistable [14–20]. In these measurements, the value of the applied current at the point where the junction switches into the voltage state is recorded many times at each temperature. Switching current measurements have been used to infer thermal activation [14, 15], quantum tunneling [15, 16], underdamped phase diffusion [17–19], and to infer the state of a quantum bit [20].

In this paper we present switching current measurements on Josephson rings. First, the current-voltage (I-V) characteristics are presented and discussed. We find that a very small voltage appears across the ring prior to switching, indicating an underdamped, low-velocity fluxon diffusion state. We also find that the switching current is different under positive and negative current, which we ascribe to the asymmetric manner in which the current is applied. Finally, the dependence of the switching current histograms on temperature is presented and analyzed in detail. We find that we can qualitatively fit the switching rate curves with the process of thermal activation over a dissipation barrier, where a low-velocity state switches to a high velocity state.

2 Measurements

2.1 Device and Measurements

The device studied was a circular array of $N = 9$ niobium-aluminum oxide-niobium Josephson junctions, fabricated at M.I.T. Lincoln Laboratory at a current density of 300 A/cm^2. A scanning electron micrograph of a device similar to the one tested is shown in Fig. 1a. Each junction is about 1.05 μm on a side (area of about 1.1 μm^2) with a critical current of about $I_{crit} = 3.3$ μA and a normal state resistance of about $R_N = 678\ \Omega$. The circular array is about 133 μm in diameter. Each of the individual 9 cells has an area of $A_{cell} = 1500$ μm^2 and an inductance of about $L = 79$ pH, calculated with FASTHENRY [21]. The normalized damping $\eta = \sqrt{\Phi_0/(2\pi I_{crit} R_N^2 C_J)}$ is about 0.06 and the normalized discreteness parameter $\lambda = \Phi_0/(2\pi L I_{crit})$ is about 1.2; here Φ_0 is the flux quantum and C_J is the junction capacitance.

The devices were cooled in a ^{3}He refrigerator and measured at temperatures of about 0.3 K to about 6 K. The voltage and current leads were filtered with copper

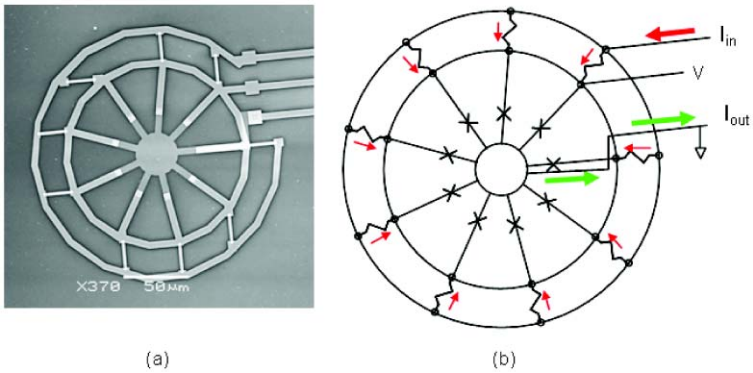

Fig. 1 Scanning electron micrograph (**a**) and schematic of the device (**b**). In the schematic, the junctions are indicated with *X*'s and the application of the current is shown. *Red arrows* indicate current entering the device while *green arrows* indicate current leaving the device

powder filters and RC low-pass filters. The device was enclosed in a copper can which was heat sunk to the ^{3}He stage. Fluxons were trapped in the ring upon cooling through the superconducting critical temperature. We could not experimentally determine the exact number of fluxons in the ring. The areas of our cells is larger than in most experiments on Josephson rings, and because of that background field fluctuations upon cool-down did not allow the necessary precision of the background flux.[1] However, only four physically different fluxon configurations are possible, those being 1, 2, 3 and 4 fluxons. In our simulations, all of these configurations give fluxon diffusion states. A saw-tooth current waveform at 100 Hz was applied to the array through a 100 kΩ bias resistor located at room temperature. In series with each junction is a 10 Ω on-chip bias resistor. Figure 1b shows the way in which the current was applied to and extracted from the device. Notice the asymmetry: current enters the device through nine separate wires, one for each junction, while current leaves the device through just one wire. This has important consequences for fluxon motion and is discussed below. The voltage across the array was measured with an instrumentation amplifier. The voltage and current waveforms were digitized directly and saved on disk. The switching currents were determined with software routines. Typically 5000 I-V curves were digitized at each temperature.

2.2 Current-Voltage (I-V) Curves

Individual I-V curves at $T = 0.35$ K and $T = 3.00$ K are shown in Fig. 2. These I-V curves look very similar to the I-V curve for a single underdamped Josephson junction. Current increases from zero along an apparent supercurrent branch and then

[1]The field increment to change the number of fluxons by one is about 10^{-3} Gauss in our device. This number is so small because of the large size of the ring. Our magnetic shield attenuation was about a factor of 20. We made an effort to control the number of fluxons, but the spurious external fields in our lab seemed to be too large, i.e. larger than 0.02 Gauss, to allow such control. We have addressed this with another layer of magnetic shielding for future experiments.

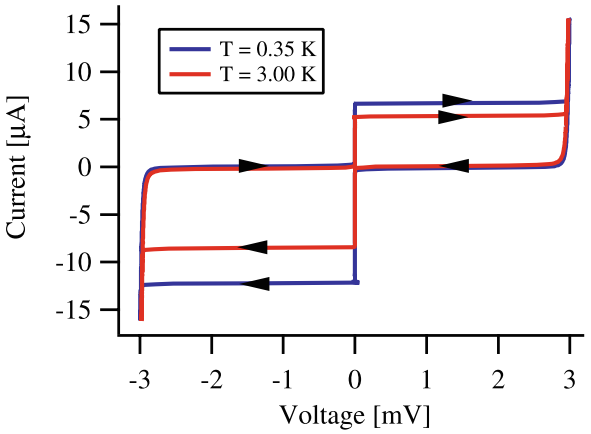

Fig. 2 Single I-V trace for the Josephson ring at 0.35 K (*blue*) and 3.00 K (*red*)

the system switches to a voltage of about 2.8 mV, the energy gap for niobium. After the current is decreased to close to zero, the system retraps back to zero voltage. The switching current is defined as the current at which the jump to the energy gap voltage occurs. As seen in the figure, lower temperatures result in larger switching currents.

In Fig. 2 one can also see that at a given temperature, the switching current is larger for negative currents than for positive currents. This was unexpected, since the junctions all have nominally the same critical current and the cells all have the same inductance. We ascribe this asymmetry to the way that we apply and extract the current. The return current comes through a single wire, as shown in Fig. 1, and this one wire carries the bias current for all nine junctions. The magnetic field from this return current puts flux of one sign in the cell to the left and flux of the other sign in the cell to the right. This flux affects the motion of the fluxon, deepening the potential well on one side and raising it on the other. We have modeled this numerically with the equations of motion for the array and find that, qualitatively, it can cause an asymmetry in the switching current.[2] We have removed this asymmetry in a new set of devices, and preliminary results show equal switching current for currents of either sign.

If we consider a Josephson ring with a fluxon trapped inside, the dynamics one would typically infer from the I-V curves of Fig. 2 are similar to that of the phase particle for a single junction. On the supercurrent branch, the fluxon is pinned in its potential minima. The energy barrier to move it to the next cell is lowered under the application of the applied current, and at the switching current the fluxon escapes and begins to move through the array, causing a voltage. The escape is triggered by thermal fluctuations in the system. Because the system is very underdamped, the moving fluxon excites a whirling mode, and all the junctions switch to the energy gap voltage. The hysteresis results because in order to retrap the fluxon, the current needs to be reduced almost to zero.

[2]Earlier experiments done by collaborators utilized a similar design, but their results did not show this effect; we believe this is because those experiments were at higher temperatures, where the currents were smaller and the dynamics were overdamped. See [22].

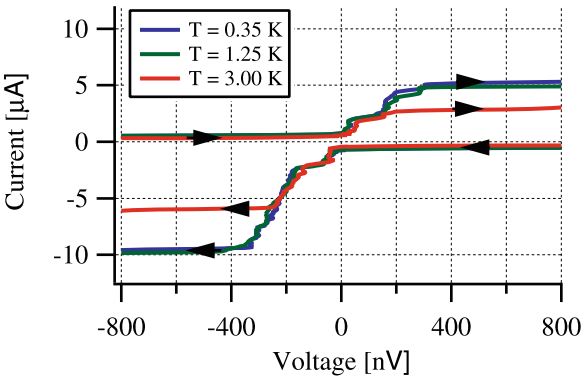

Fig. 3 Zoom-in of the average I-V curve for 0.35 K, 1.25 K, and 3.00 K. The voltage across the array is in the 200–300 nV range before switching and indicates the presence of low-velocity fluxon motion

However, this picture is not exactly correct in our device. In Fig. 3 we show I-V curves at 0.35 K, 1.25 K and 3.00 K, but with the voltage axis expanded significantly. Here the I-V curves have been averaged 5000 times to reduce electronic noise. Now we can see that the apparent supercurrent branch is actually at a very small voltage, of order hundreds of nV. This is an important observation, because it indicates that the fluxon escapes not from a stationary state, but rather from a dynamic state.

We have recently explored the physics of this low-voltage state in a computational study [23]. This state is characterized by a non-zero mean velocity of the fluxon, where it moves by a series of noise-induced phase slips. We term this motion fluxon diffusion, in analogy with the underdamped phase diffusion that occurs in a single junction. Like underdamped phase diffusion, fluxon diffusion occurs in an underdamped, hysteretic system [24]. Unlike underdamped phase diffusion, however, fluxon diffusion does not need frequency-dependent damping to occur. In this paper we are not able to compare our experimental results directly to our numerical simulations due to the asymmetry in current application, described above. However, we can confirm the presence of fluxon diffusion in our data by the observation of the low voltage prior to switching (Fig. 3) and the analysis of the switching data (see below).

2.3 Switching Current Measurements

For each I-V curve measured, a switching current was determined at a voltage threshold of (+1 mV) for positive current and (−1 mV) for negative current. The retrapping currents were computed in a similar way. At each temperature we measured 5000 switching currents and retrapping currents. Figure 4 shows the histograms for four different temperatures: 0.35 K, 1.25 K, 3.00 K and 5.18 K. Also shown is a histogram of the retrapping events at 3.00 K. Here, and for the other switching current data and analysis, we have presented results for only negative applied currents for brevity. Results for positive applied currents gave similar results as those for negative applied currents except with different fitting parameters, which we indicate when appropriate.

The width of the retrapping histogram in Fig. 4 is extremely narrow, as the process of retrapping has intrinsically much smaller fluctuations than the process of switching. We have not yet explored the physics of the retrapping process in our devices, but

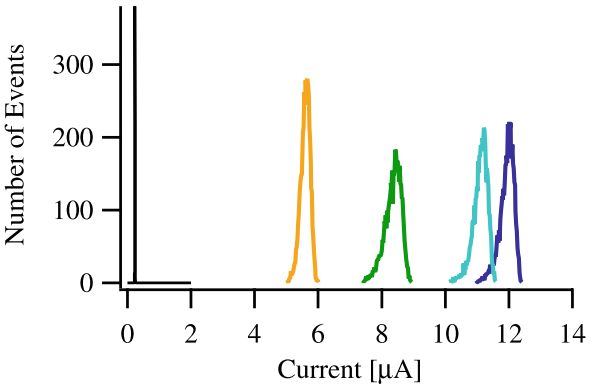

Fig. 4 Histograms of the retrapping current at 3.00 K (*black*) and for the switching current at 0.35 K (*purple*), 1.25 K (*blue*), 3.00 K (*green*), and 5.18 K (*yellow*). The value of dI/dt was 6000 μA/s

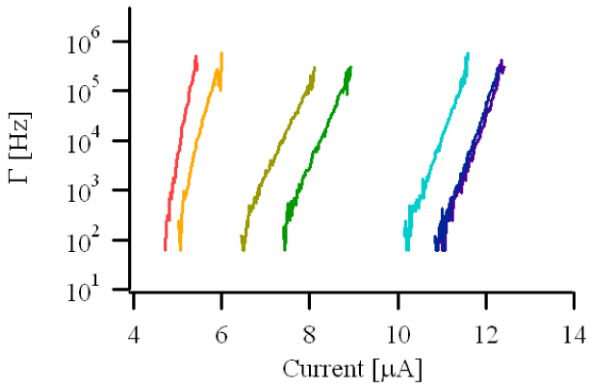

Fig. 5 Switching rate (Γ) versus applied current for 7 different temperatures. The temperatures are, from *right* to *left*: 0.35 K, 0.55 K, 1.25 K, 3.00 K, 3.50 K, 5.18 K, 5.58 K. The rate shows an exponential dependence on current

for now we use it as a measure of experimental uncertainty due to electrical noise or other external sources. From the narrow width of the retrapping histogram in Fig. 4 we conclude that the experimental uncertainty is very small; we would not be able to measure such a narrow histogram otherwise.

The shapes of the switching histograms are reminiscent of switching in single junctions, either through thermal activation or quantum tunneling, with slightly more events at currents below the peak of the histogram than above the peak. We convert the histogram data into a switching rate per unit time Γ, using the procedure first introduced by Fulton and Dunkleberger [7–9]. The experimental ramp rate was $(dI/dt) = 6000$ μA/s. Rate curves as a function of current are shown for 7 different temperatures (0.35 K, 0.55 K, 1.25 K, 3.00 K, 3.50 K, 5.18 K and 5.58 K) in Fig. 5. They show the expected exponential dependence on current. Finally, in Fig. 6 we show the average switching current, $\langle I_{sw} \rangle$, and standard deviation, σ_{Isw}, for each distribution as a function of temperature. These data will be used in analyzing the rate curves below.

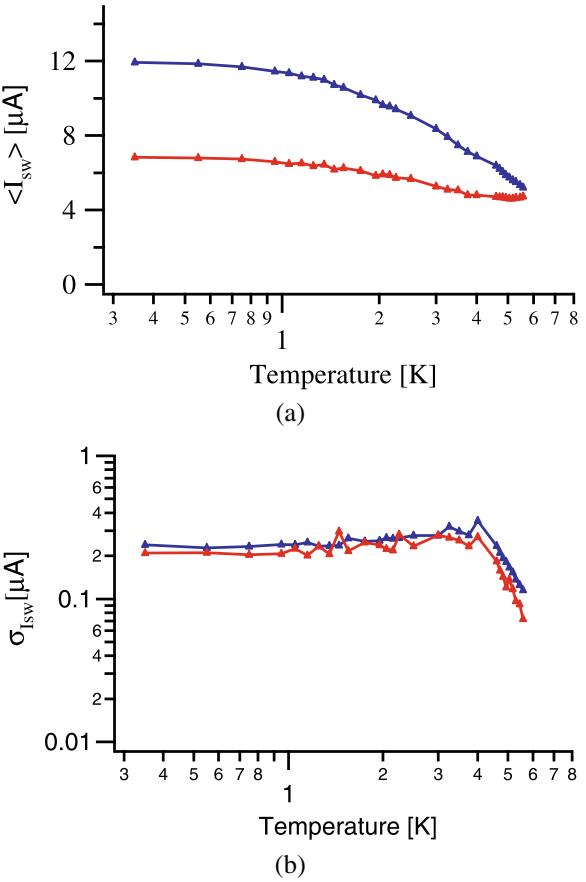

Fig. 6 Switching current average (**a**) and standard deviation (**b**) as a function of temperature. *Blue* indicates the minus direction and *red* indicates the plus direction

3 Analysis of Switching Current Measurements

In this section we analyze the switching current data and its temperature dependence. We are specifically interested in understanding the rate curves from Fig. 5 with the process of switching from a low-velocity state to a high-velocity state.

We follow the work of Vion et al. [25], who study such a process in a Josephson system. Their device is a single Josephson junction of critical current I_0 biased in series with an on-chip resistor (R) and in parallel with an on-chip capacitance (C). A circuit model is shown later in Fig. 11c. At low bias currents, the junction is in a low-velocity, phase-diffusion state. At the switching current, the junction is thermally excited from this diffusion state to the high-voltage running state. In order to reach that voltage, the external RC circuit must be charged and energy must be dissipated; thus a "dissipation barrier" separates the two states.

After normalizing the equations of motion, the dynamics of their system are mapped to an effective Langevin equation. The new coordinate in this normalization is proportional to the phase velocity. The rate Γ to switch to the running state is given by a *static*, over-damped Kramers rate; the switching condition is when the system

reaches a critical velocity and escapes from the low-velocity state to the high-velocity state. The rate is specified by (3)–(5) in Vion et al. [25]. For ease of comprehension, we use the following expression for Γ:

$$\Gamma = \left(\frac{11\omega_J}{2\pi\alpha}\right)\left(1-\frac{I}{I_{\max}(T)}\right)^{1/2}\exp\left[-\frac{\alpha E_J}{6kT}\left(1-\frac{I}{I_{\max}(T)}\right)^{3/2}\right]. \quad (1)$$

Equation (1) was empirically determined by computing the value of Γ at different temperatures and currents from (5) in Vion et al. Here $\omega_J = 2\pi R I_0/\Phi_0$ is the junction frequency, $\alpha = 2\pi R^2 I_0 C/\Phi_0$ is the dissipation factor, $E_j = \Phi_0 I_0/(2\pi)$ is the Josephson energy, k is Boltzmann's constant and T is temperature. $I_{\max}(T)$ is the temperature-dependent maximum current for which the dissipation barrier still exists, equal to $\max[S(u)]$ in Vion et al. [25]; currents greater than $I_{\max}(T)$ result in definite switching. The arguement in the exponential in (1) matches the expressions in Vion et al. to 5% or better in the range of switching currents and temperatures studied. The pre-factor does not match quite as well (about 50% or better), but the pre-factor does not affect our results significantly.

Writing the rate in the form of (1) allows us to now use the general formalism developed by Garg [26], who computes the switching rate that results from the first escape out of a potential minima. Here the rate Γ is defined as follows:

$$\Gamma = A\left(1-\frac{I}{I_c}\right)^{a+b-1}\exp\left[-B\left(1-\frac{I}{I_c}\right)^{b}\right]. \quad (2)$$

Equation (2) is a general expression that applies to switching in a Josephson junction with critical current I_c. A, B, a and b are constants which depend on temperature and damping. It is easily seen that (1) and (2) are equivalent for $I_c = I_{\max}$, $a = 0$, $b = 1.5$, $A = 11\omega_j/(2\pi\alpha)$ and $B = \alpha E_j/(6kT)$. Equations (7) and (8) in Garg [26] also gives expressions for the average, $\langle I_{sw}\rangle$, and standard deviation, σ_{Isw}, of a switching current distribution in terms of a, b, A, B and I_c. To plot (2) in a manner that is equivalent for all temperatures, we define the rescaled current as:

$$Z = B\left(1-\frac{I}{I_c}\right)^{b}, \quad (3)$$

and the rescaled rate as:

$$F = \ln\left[\frac{\Gamma}{A\,(1-I/I_c)^{a+b-1}}\right]. \quad (4)$$

Using these definitions, (2) can then be written as:

$$F = -Z. \quad (5)$$

Thus, curves for different temperatures should all fall onto the same curve defined in (5) provided the correct values of a, b, A, B and I_c have been used at each temperature.

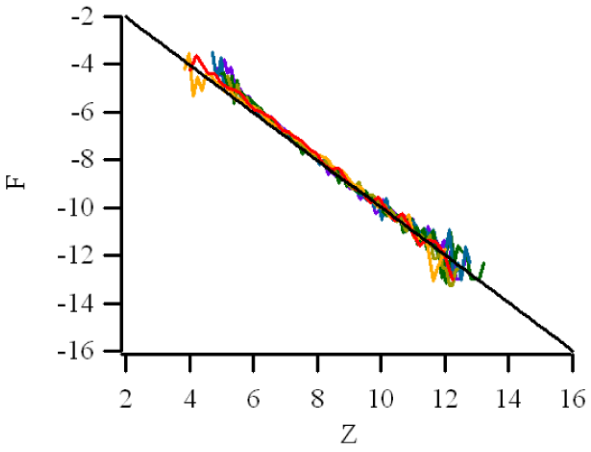

Fig. 7 Normalized rate (F) versus normalize current (Z) for the same seven rate curves in Fig. 5. Color coding is the same as in Fig. 5

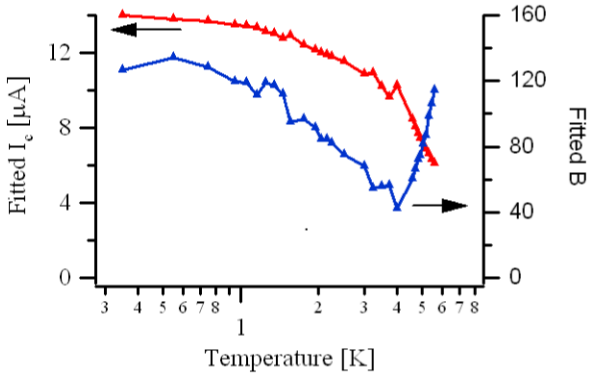

Fig. 8 Fitted I_c (*left axis*) and B (*right axis*) versus temperature. The lines are a guide to the eye. Deviations from the theory occur at temperatures above 5 K, where it can be seen that the fitted B coefficient starts to increase and the fitted I_c starts to decrease more sharply

We analyze the rate curves in Fig. 5 by first finding the Garg parameters B and I_c that scale all of the curves onto the form given by (5), and then comparing them to what we expect from (1). First, as suggested by (1), we choose $b = 1.5$, $a = 0$ and hold A at a constant value for all temperatures. Then, we use the measured values of $\langle I_{sw} \rangle$ and σ_{Isw} at each temperature (Fig. 6) to choose values for B and I_c. This is done by numerically back-solving for B and I_c using the expressions in Garg [26] for $\langle I_{sw} \rangle$ and σ_{Isw}. Overall, what we have done with this procedure is to use (2) to convert our measurements of $\langle I_{sw} \rangle$ and σ_{Isw} into measurements of B and I_c, which are parameters that have more physical meaning.

The results are shown in Figs. 7 and 8. In Fig. 7, we show the results of the scaling. All seven temperatures shown in Fig. 5 now collapse onto the same curve. The values of I_c and B needed to obtain this scaling are shown in Fig. 8. As best as we could tell, no other set of parameters scaled the curves in a similar fashion. These fitted values did not depend sensitively on the value of A. The value of A used was 5.7×10^7 Hz; this was chosen to be consistent with the junction frequency ω_J, discussed below.

We now compare these fitted values of the parameters in terms what is expected from Vion et al. Incidentally, it is clear immediately that thermal activation or quan-

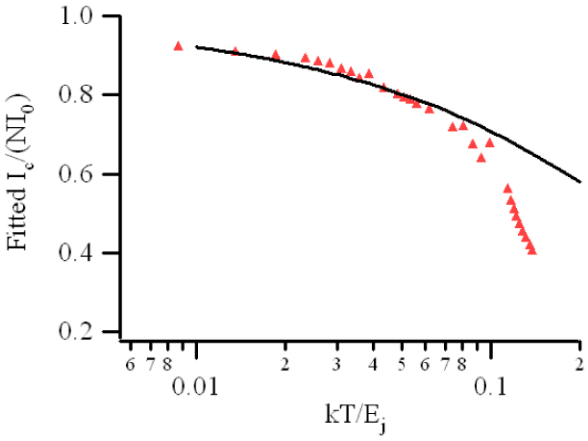

Fig. 9 Fitted I_c normalized to NI_o (*triangles*) versus normalized temperature (kT/E_j). *Black line* is the curve $I_{\max}(T)$ calculated from Vion et al.

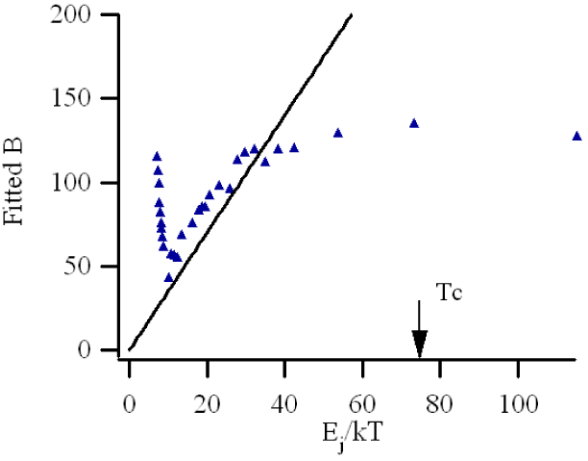

Fig. 10 Fitted B (*triangles*) versus E_j/kT. The *black line* is a fit with $\alpha = 21$. The single-junction quantum transition temperature is indicated at E_j/kT equal to 73

tum tunneling from a stationary state do not describe our system, since the fitted I_c depends on temperature. (This is also clear since the standard deviation does not increase with increasing temperature.) In switching from a dynamic state, however, the maximum current $I_{\max}$ does depend on temperature, since thermal fluctuations affect the height and shape of the dissipation barrier. In Fig. 9 we compare the temperature dependence of the fitted critical current with the temperature dependence of $I_{\max}$, calculated using the expressions in Vion et al. Only one fitting parameter, I_0, is used. This parameter scales *both* axes of Fig. 9: the applied current is scaled as $I/(NI_0)$ and the temperature is scaled as kT/E_j, where E_j is proportional to I_0. We see that the temperature dependence of our fitted I_c is very consistent with $I_{\max}(T)$ for a dissipation barrier. A fitted value of $I_0 = 1.7$ μA was used in Fig. 9. For positive applied current, a value of $I_0 = 1.12$ μA best fits the data.

We next look at the fitted values of the B coefficient. In Fig. 10 we plot B versus $E_j/(kT)$. Using $B = \alpha E_j/(6kT)$ from (1), we find that $\alpha = 21$ fits the data in

the linear range. Deviations from this expected linear relationship occur at both low temperatures and at high temperatures; this is discussed below.

4 Discussion

We have performed measurements of switching current distributions on 9-junction Josephson rings at low temperatures. The rings are highly underdamped, resulting in bistability in the I-V curves. A small voltage, of order hundreds of nanovolts, is measured across the junction before the jump to the voltage state. Histograms of switching current data are qualitatively consistent with the process of thermal activation over a dissipation barrier as described by Vion et al. [25], where a low-velocity state switches to a high-velocity state. These two observations both indicate the presence of low-velocity fluxon diffusion before switching. To the best of our knowledge, fluxon diffusion in an underdamped, hysteretic system has not been experimentally observed previously.

In our array, including the bias resistors, there are 27 degrees of freedom—the phase, junction voltage and bias-resistor voltage for each of the 9 junctions. Since we have not made an effort to control the environmental impedance of the leads, a 28th degree of freedom can be added to represent the effective RC-shunt caused by the environment. Figure 11a shows this circuit model. When studying the dynamics of a fluxon in a Josephson array, it is very common to use the picture of a single particle to represent this extended and collective object. The fluxon's dynamics are represented as that of a damped particle in a periodic, tilted potential (Peierls-Nabarro potential)—in effect, a single Josephson junction. This is indicated in Fig. 11b. This collapses the many degrees of freedom in the array onto just two, phase and velocity.

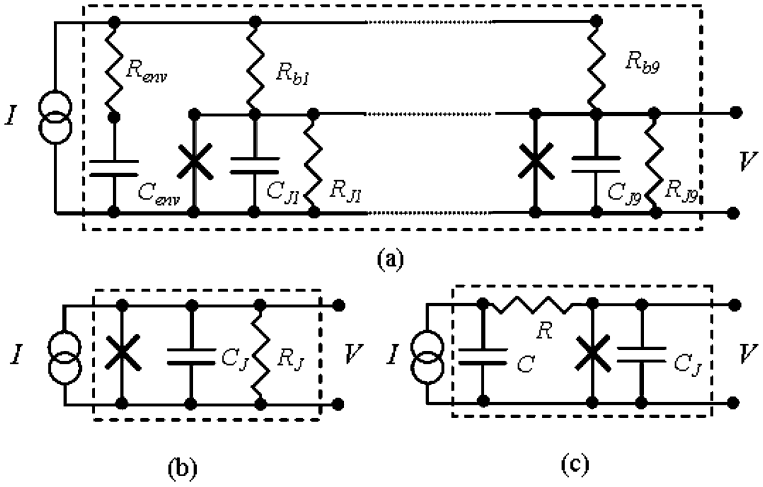

Fig. 11 Circuit models for the complete array with environmental impedance (**a**), the typical single-particle picture (**b**), and the model of Vion et al. (**c**). The *boxes with the dashed lines* isolate the measured I and V. Note that the resistor and capacitor in model (**c**) are meant to be part of the array dynamics, not external components

In many situations this does indeed preserve much of the dynamics. Clearly, such a simplification would be useful in our case.

However, as pointed out by Kautz and Martinis [24], the combination of diffusion and hysteresis is not possible in a single-junction model with two degrees of freedom. In many cases, extra degrees of freedom are effectively added to the circuit due to the impedance of the bias leads. We have numerically found in [23] that fluxon diffusion and hysteresis exist in the ring without the inclusion of extra evironmental degrees of freedom. The model of Vion et al. adds a third degree of freedom, the voltage across the resistor R, but now allows this combination. This model is shown in Fig. 11c. Our work in this paper has been to show that when the fluxon's dynamics includes diffusion, they can be approximated onto this model. It is important to realize that in this representation, the R and C are not external circuit parameters but rather are part of the array; the dotted boxes in the figure indicate how the two models coincide. In the case where fluxon diffusion is present, one might argue that this is the simplest model possible and should replace the single-particle picture.

We now discuss the physical significance of fitting parameters I_0 and α, and how they map on the circuit parameters R and C of Vion et al. We expect the fitted critical current $I_0 = 1.7$ μA to be equal to the zero-temperature switching current of the fluxon, the current where the fluxon excites a whirling mode after its initial escape. In a single junction, this represents the minimum current for which the potential energy gain of the phase particle starting at the top of a well offsets the frictional losses after moving down the well; in the notation of Kautz and Martinis, this current is termed i_m [24]. For a fluxon in a parallel array, this current depends on many factors: the radiative damping of the fluxon, the number of fluxons trapped in the array, and, in our case, the extra flux due to the return lead. Our lack of knowledge of some of these factors prevented a precise calculation of this current. However, some intuition can still be applied. We can say that I_0 should not be smaller than the fluxon depinning current (about 0.13 μA) and should not be larger than the critical current of the junctions in the ring ($I_{crit} = 3.3$ μA). The frictional losses due to the environmental impedance also set a lower bound on this number. The real part of the impedance at the junction frequency, approximately equal to R_{env} in Fig. 11a, is the key parameter. This value is not well characterized in our setup, as it depends on how the resistance and capacitance of the measurement lines are distributed, but should be somewhere between 10 Ω and 200 Ω. Assuming a value in the middle of that range ($R_{env} = 100$ Ω) gives a depinning current of 0.44 μA, using (39) in Kautz and Martinis [24]. The radiation damping of the fluxon should certainly make the switching current larger than that, so the fitted values of 1.12 μA and 1.7 μA seem reasonable.

In Fig. 10, we find that the data in the range of $E_J/kT = 15$ to 40 is well-described by a single value of α, but that there are deviations from a linear relationship above and below these temperatures. The deviations of the model at high temperatures (low values of E_J/kT) are also present in the fitted I_c in Fig 9. From this, it is clear that the simple model does not work as well at these temperatures, starting at around 5 K or so (see Fig. 8). These deviations can be possibly be explained by the fact that the model of Vion et al. does not account for dissipation in the junction itself, but rather only in the external R and C (see Fig. 11c). In the case of the array, the dissipation in the individual junctions increases significantly starting at 5 K: the retrapping current

starts to increase and the energy-gap voltage starts to decrease. It is possible that the value of α may need an additional contribution at these higher temperatures to account for this increased dissipation.

Meanwhile, at the lowest 3 or 4 temperatures studied (highest values of E_J/kT), the fitted B coefficient levels off, causing the apparent value of α to decrease. This discrepancy remains unexplained and will be the subject of future work. It is possible that quantum tunneling plays a role here, as the crossover temperature for the individual junctions in the array is equal to 0.55 K, or E_J/kT equal to about 73. This crossover temperature is indicated in Fig. 10. However, the effect of tunneling on fluxon diffusion has not yet been studied, so both more theoretical and experimental work is needed here.

Finally, to complete the circuit model in Fig. 11c, we choose the values of R and C which best reproduce the fluxon dynamics. The value of R is chosen to match the diffusion voltage of the array before switching. Using the equations in Vion et al., we find that at 0.35 K the voltage across the junction is about $1.6I_0R$ before switching. From Fig. 3, we see that this voltage is about 400 nV; this leads to a value of R of 0.15 Ω. This value of R can be used to calculate the junction frequency, ω_J; we find that $\omega_J = 0.77$ GHz. Since the diffusion voltage is of order I_0R, this frequency is approximately equal to the fluxon "jump" frequency $2\pi V/\Phi_0$ in the diffusion state. Depending on the definition of the center of mass of the fluxon, the fluxon's velocity in the diffusion state is either ω_J or $N\omega_J$. Meanwhile, the overdamped dynamics in the diffusion state are characterized by the fitted value of $\alpha = 21$; this give a value of $C = 169$ nF. Recall again that C does not correspond to an actual on-chip capacitor, but is a more phenomenological parameter to represent the fluxon dynamics. Our future work will focus on trying to understand these parameters better from the point of view of the physics of the array.

Acknowledgements Work is partially supported by DGICYT through project FIS2005-00337 (J.J.M) and through NSF DMR 0509450 (K.S.).

References

1. S.H. Strogatz, *Nonlinear Dynamics and Chaos* (Perseus Books, New York, 1994)
2. K.K. Likharev, *Dynamics of Josephson Junctions and Circuits* (Gordon and Breach, New York, 1986)
3. J.J. Mazo, T.P. Orlando, Chaos **13**, 733 (2003)
4. R.S. Newrock, C.J. Lobb, U. Geigenmüller, M. Octavio, Solid State Phys. **54**, 263 (2000)
5. J.J. Mazo, J.C. Ciria, Phys. Rev. B **54**, 16068 (1996)
6. E. Trías, J.J. Mazo, T.P. Orlando, Phys. Rev. B **65**, 054517 (2002)
7. S. Watanabe, H.S.J. van der Zant, S.H. Strogatz, T.P. Orlando, Physica D **97**, 429 (1995)
8. A.V. Ustinov, M. Cirillo, B.A. Malomed, Phys. Rev. B **47**, 8357 (1993)
9. F. Falo, P.J. Martínez, J.J. Mazo, T.P. Orlando, K. Segall, E. Trías, Appl. Phys. A **75**, 263 (2002)
10. O.M. Braun, Y.S. Kivshar, Phys. Rep. **306**, 1 (1998)
11. L.M. Floria, J.J. Mazo, Adv. Phys. **45**, 505 (1996)
12. S. Watanabe et al., Physica D **97**, 429 (1995)
13. A.V. Ustinov, Physica D **123**, 315 (1998)
14. T.A. Fulton, L.N. Dunkleberger, Phys. Rev. B **9**, 4760 (1974)
15. A. Wallraff, A. Lukashenko, C. Coqui, A. Kemp, T. Duty, A. Ustinov, Rev. Sci. Instrum. **74**, 3740 (2003)
16. J.M. Martinis, M.H. Devoret, J. Clarke, Phys. Rev. B **35**, 4682 (1987)

17. J. Mannik, S. Li, W. Qiu, W. Chen, V. Patel, S. Han, J.E. Lukens, Phys. Rev. B **71**, 220509 (2005)
18. V.M. Krasnov, T. Bauch, S. Intiso, E. Hurfeld, T. Akazaki, H. Takayanagi, P. Delsing, Phys. Rev. Lett. **95**, 157002 (2005)
19. J.M. Kivioja, T.E. Nieminen, J. Claudon, O. Buisson, F.W.J. Hekking, J.P. Pekola, Phys. Rev. Lett. **94**, 247002 (2005)
20. I. Chiorescu et al., Science **299**, 1869 (2003)
21. M. Kamon, M.J. Tsuk, J.K. White, IEEE Trans. Microwave Theory Tech. **42**, 1750 (1994)
22. E. Trias, J.J. Mazo, T.P. Orlando, Phys. Rev. E **61**, 2257 (2000)
23. J.J. Mazo, F. Naranjo, K. Segall, Phys. Rev. B (to appear). http://arxiv.org/abs/0806.4828
24. R.L. Kautz, J.M. Martinis, Phys. Rev. B **42**, 9903 (1990)
25. D. Vion et al., Phys. Rev. Lett. **77**, 3435 (1996)
26. A. Garg, Phys. Rev. B **51**, 15592 (1995)